Influence of Plasma Surface Treatments on Kink Band Formation in PBO Fibers During Compression

Eduardo Lorenzo-Villafranca,[1] Katia Tamargo-Martínez,[1] Jon M. Molina-Aldareguia,[1] Carlos González,[1,2] Amelia Martínez-Alonso,[3] Juan M. D. Tascón,[3] Mercedes Gracia,[4] Javier Llorca[1,2]

[1]*Instituto Madrileño de Estudios Avanzados de Materiales (Instituto IMDEA Materiales), C/Profesor Aranguren s/n, 28040 Madrid, Spain*
[2]*Departamento de Ciencia de Materiales, Universidad Politécnica de Madrid, E. T. S. de Ingenieros de Caminos. 28040 Madrid, Spain*
[3]*Instituto Nacional del Carbón (INCA-CSIC), Apartado 73, 33080 Oviedo, Spain*
[4]*Instituto de Química-Física "Rocasolano" (IQFR-CSIC), Serrano 119, 28006 Madrid, Spain*

Received 11 January 2011; accepted 28 March 2011
DOI 10.1002/app.34568
Published online 23 August 2011 in Wiley Online Library (wileyonlinelibrary.com).

ABSTRACT: The effect of nitrogen and oxygen plasma surface treatments on the compressive strength of PBO fibers has been studied. To this end, the nucleation and propagation of compression-induced kink bands was carefully monitored by means of *in situ* bending tests inside a scanning electron microscope. The micromechanisms of deformation were identical irrespective of fiber surface condition (either as-received or modified by plasma) but the critical stress necessary to induce irreversible damage in compression in the nitrogen-plasma treated fibers was 40% higher than in the as-received fibers. This improvement occurred without any reduction in the fiber tensile properties. The source of this behavior is discussed in the light of the morphological and chemical changes induced by the plasma treatments on the fiber surface, as studied by AFM and XPS. © 2011 Wiley Periodicals, Inc. J Appl Polym Sci 123: 2052–2063, 2012

Key words: fibers; high performance polymers; compression; surface modification; electron microscopy

INTRODUCTION

Poly *p*-(phenylene benzobisoxazole) or PBO (Fig. 1) polymeric fibers present outstanding specific mechanical properties (particularly tensile strength and modulus) that make them suitable for structural applications in which weight is a critical issue. However, PBO fibers tend to fail prematurely in compression due to the formation and propagation of kink bands,[1–4] and this phenomenon hinders their use in structural components subjected to compressive stresses as well as to fatigue. In general, kink bands act as a potential failure mode for highly anisotropic fibers such as aramids, poly[diimidazo pyridinylene dihydroxy-phenylene] or PIPD, poly(*p*-phenylene benzobisthiazole) or PBZT, carbon, etc., in which the lateral interactions between the aligned polymeric chains are very weak (hydrogen bonds or Van der Waals forces).[5–7]

The micromechanisms of kink band formation in PBO fibers have been studied previously[1,8–10] to improve the compressive properties of rigid-rod polymeric fibers.[11–15] However, the process of kink band initiation and propagation is not yet fully understood and improvements in the compressive strength of PBO are usually accompanied by a marked degradation of the corresponding tensile properties (of the order of 25%).[11,14,15] The most widely accepted theories establish that compressive failure by kink band formation occurs due to an elastic microbuckling instability of the polymeric fibrils[16] or due to a shear instability.[17] In any case, the kink band is initiated on the surface and propagates through the fiber cross-section as the strain increases[11] due to the weak interaction between the aligned polymeric chains. Modifications of the fiber surface, particularly by increasing the crosslink density between polymeric chains, should constitute a suitable strategy to alter the conditions for the formation of the kink band and hence the compressive fiber strength.

Among the different surface modification techniques available, plasma treatments offer the capability of changing the surface physical and chemical

Correspondence to: J. M. Molina-Aldareguia (jon.molina@imdea.org).

Contract grant sponsor: Spanish Ministry of Science and Innovation through the program TRACE; contract grant number: TRACE PET2008_0315.

Contract grant sponsor: Future Fibers Rigging Systems S.L. within the framework of the project FUTURE-PBO.

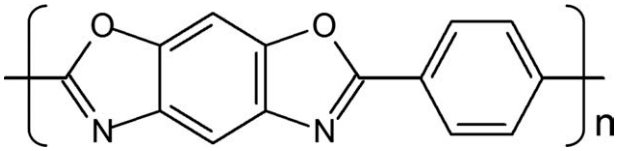

Figure 1 Monomer unit of PBO fiber.

properties without modifying the bulk material. Thus, polymer surface properties (wettability, chemical composition, and roughness) can be tailored by controlling the experimental parameters of the plasma treatment (power, time, pressure, and gas composition).[18] Although it is difficult to predict the extent of the depth affected by the treatment because several processes can take place simultaneously (ablation, branching, and/or crosslinking), the modifications are usually confined to the uppermost layers of the material.[18] For instance, previous work[19,20] has shown that oxygen and nitrogen plasma treatments improve the adhesion of PBO fibers to epoxy resins, without degradation of the tensile properties. Nevertheless, the compressive properties of the individual filaments were not studied, and this investigation is focused on the effect of oxygen and nitrogen plasma treatments in the compressive properties of PBO fibers and the corresponding mechanisms of kink band formation.

To this end, the deformation of treated and untreated PBO fibers in bending was *in situ* monitored inside a scanning electron microscope (SEM). This technique allows the direct observation of the process of kink band initiation and propagation as a function of the applied strain. In addition, the fiber tensile strength was determined before and after the bending tests to study the effect of kink bands on the degradation of the axial properties. The results showed large differences in the critical strain for irreversible damage due to kink bands depending on the particular surface plasma treatment, which did not lead to the degradation of the tensile fiber strength. These results are discussed in the light of the topographical and chemical changes induced by the plasma treatments, as obtained by X-ray photoelectron spectrometry (XPS) and atomic force microscopy (AFM) studies.

EXPERIMENTAL

The PBO fibers studied were extracted from Zylon® HM fiber yarns supplied by Toyobo (referred to as sample Z). The filament diameter, as reported in the manufacturer's datasheet, was approximately 11.6 μm, and the specific linear density was 545 dtex. The plasma surface modification was carried out in a microwave reactor (Technics Plasma, model 200-G) using a power of 70 W for 4 min. As-received PBO fibers were modified using two treatment gases, oxygen and nitrogen, and the corresponding gas pressure inside the reaction chamber was 1.0 mbar. The plasma-treated materials are referred to as ZO4 (oxygen treatment) and ZN4 (nitrogen treatment).

The axial compressive strain in the fiber surface which led to the initiation and propagation of kink bands was determined by means of bending tests inside the SEM. Short fiber segments were glued with cyanoacrylate (superglue®) on a cardboard frame for easy handling and mounting. The shape and dimensions of the experimental fixture are shown in Figure 2. The cardboard frame had a central window of 2 mm in length. The specimens were coated with Au by sputtering (Emitech K 550X) to avoid charging effects and to enhance the quality of the SEM observations. Mechanical tests were carried out using an electromechanical testing machine (Kammrath and Weiss GmbH, Dortmund, Germany) inside a Zeiss EVO MA15 SEM operated at 3 kV. The ends of the cardboard frame were connected to the mechanical testing machine and bending of the fibers was achieved by bringing together the two ends of the fiber using the step motor of the mechanical testing machine. Elastic buckling of the slender fiber occurred at very low strain and the fiber deformed by bending. Micrographs were taken at different magnifications during the process to assess the onset and propagation of the kink band as a function of the applied strain. They were obtained at two different tilts to follow the in-plane as well as the out-of-plane displacements of the fiber during bending. To understand in more detail the process of kink band formation, some of the bent fibers were cut longitudinally using a FEI Quanta dual-beam FIB workstation and the longitudinal cross-section observed by SEM.

Tensile tests were carried out on single fibers following the ASTM D 3379 75 standard ("Standard test method for Tensile Strength and Young's modulus for High-Modulus Single-Filament Materials") to check the effect of the plasma surface treatments on the tensile strength. Instead of using the average diameter of the fibers (as specified in the standard), the diameter of each tested fiber segment was determined by SEM to provide more accurate values of the tensile strength and modulus.

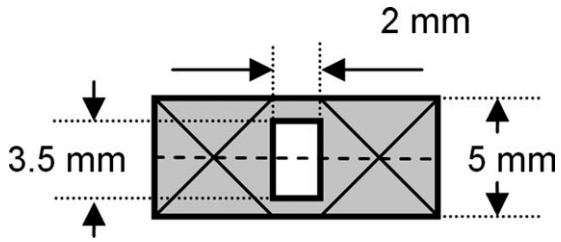

Figure 2 Experimental fixture for the bending tests.

The surface chemical changes induced by the plasma treatment were studied by XPS. XPS spectra were recorded on a CLAM2/4S (Fisons) spectrometer with an AlK_α source and an operating vacuum pressure below 3×10^{-8} mbar. The spectra were recorded at take-off angles of 90° from the samples rolling up on a polished copper plate (Cu-holder-plate). Survey spectra were obtained for elemental quantification purposes and high resolution spectra allowed the analysis of the chemical state of the elements (C, N, and O) on the fiber surface. Several spectra were recorded for each sample and also on different samples for each fiber. A constant analyzer transmission energy of 100 eV for the survey spectra and of 20 eV for the narrow scan spectra were used. The survey spectra were recorded between 1 and 1000 eV and the high-resolution spectra were acquired in the range 280–302 eV for C1s, 390–405 eV for N1s, and 524–548 eV for O1s. Charging of the samples, as a result of photoemission, was corrected using the C—C component of C1s signal at 284.6 eV as an internal standard.[21] Shirley background was used to correct the XPS spectra and intensities were converted to elemental concentrations using Wagner sensitivity factors (0.25, 0.42, and 0.66 for C1s, N1s, and O1s, respectively[22]).

Finally, the morphology changes induced by the plasma treatment were studied by AFM under ambient conditions (relative humidity $\sim$ 45%, temperature $\sim$ 22–23°C) and using rectangular silicon cantilevers (spring constant $\sim$ 40 N m^{-1}, resonance frequency around 250 kHz). AFM phase images were obtained in tapping mode operated in the attractive interaction regime. The free (A_0) and set-point (A_{sp}) amplitudes were determined from phase-distance curves being 15–30 nm the values adopted for A_0 and 0.8–0.9 for rsp (rsp $= A_{sp}/A_0$).[20]

RESULTS

PBO bending studies inside the SEM

A large number of tests was carried out in the as-received fibers to understand the process of damage formation during bending. At each loading stage, the curvature of the fibers was measured from the SEM micrographs. All fibers displayed the same sequence of events, as schematically reported in Figures 3 and 4. A large number of regularly spaced kink bands developed when the curvature was very low. They started in the compression side of the fiber and formed an angle in the range 60°–70° with fiber axis, as shown by the arrows in Figure 3. Two sets of kink bands can be observed to each side of the fiber center with opposite angles of inclination (see right part of the Fig. 3(c) micrograph). At this stage of deformation, the fiber bends uniformly along its length and can be bent back and forth without further damage. Even more, the kink bands seemed to disappear on unbending, showing the reversibility of the kink-band formation process, as pointed out in other studies.[23] Several fibers bent up to this point were tested in tension and no degradation of the tensile strength was found, indicating that this type of kink bands do not lead to permanent damage.

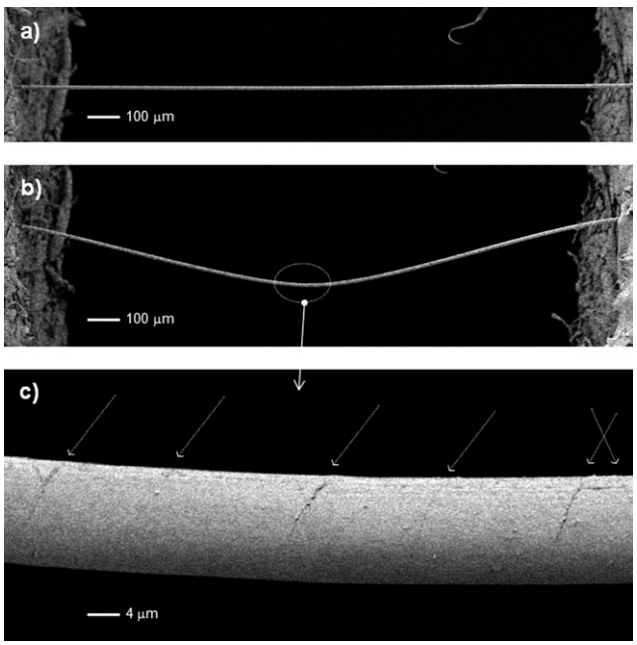

Figure 3 SEM micrographs obtained before (a) and during bending at different magnifications (b,c). The arrows indicate the location and inclination of the kink bands.

The number of kink bands increased with the bending curvature (i.e., the spacing between kink-bands was reduced) until two kink bands with opposite orientation intersected around the fiber center, as shown in Figure 4(a), producing a "V" shape defect. From now on, we will refer to the intersecting kink bands as a knuckle. Contrary to the behavior of isolated kink bands, the formation of the knuckle represents an irreversible damage process that has a strong influence on the behavior of the PBO fiber.

The fiber curvature was not homogeneous any more once the knuckle was formed, and the fiber segments at each side of the knuckle remained approximately straight, while the bending strain was completely localized at the knuckle, as shown in Figure 4(b,c). This was accomplished by the formation of multiple intersecting kink-bands in the knuckle, as can be readily observed in Figure 4(c). Furthermore, the knuckle did not disappear on unbending and all the strain was localized at the knuckle if the fiber was bent back and forth, contrary to the homogeneous deformation observed in pristine PBO fiber segments. Finally, the tensile strength of the fiber

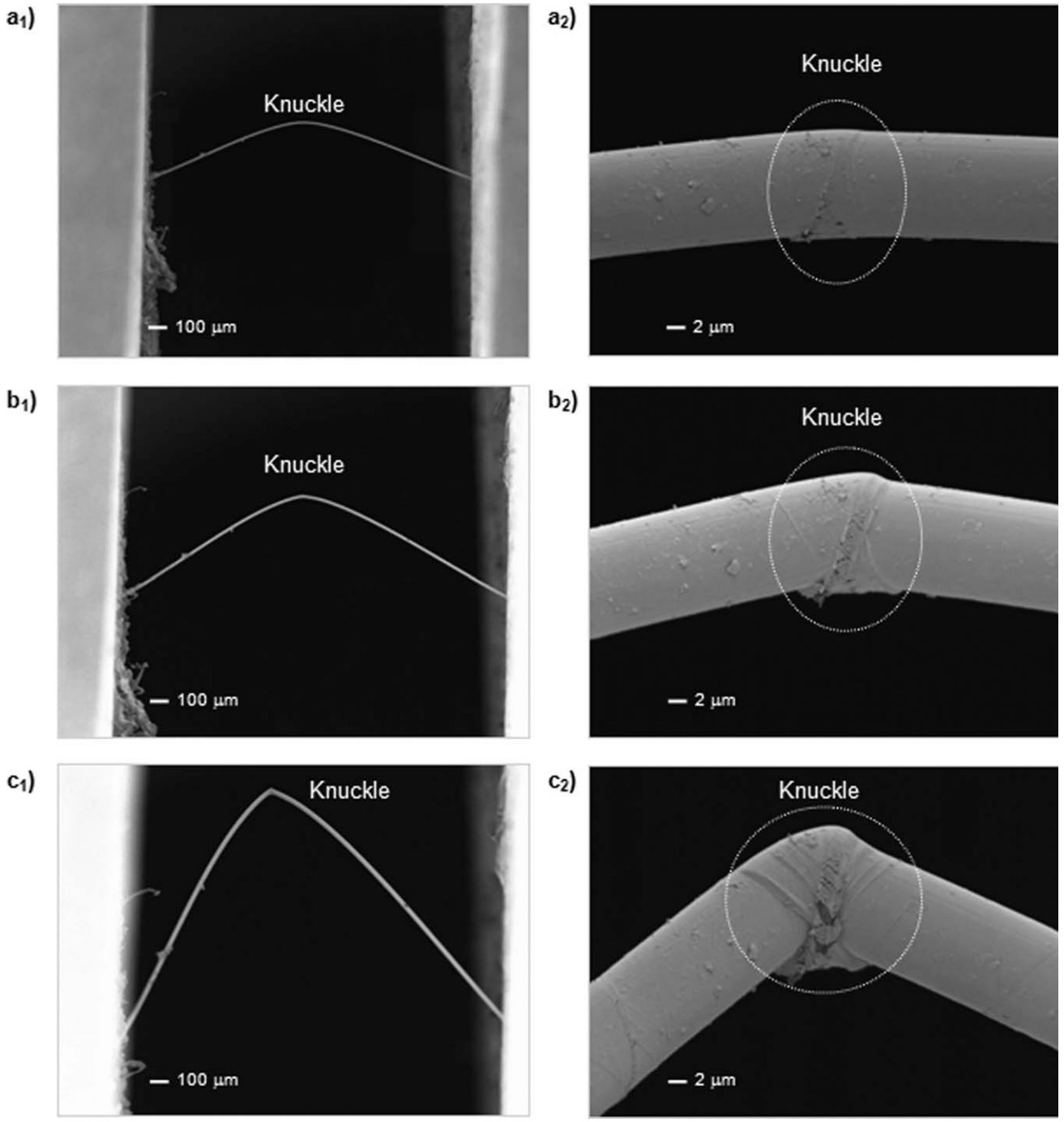

Figure 4 The sequence a–c represents the formation of a knuckle in a PBO fiber subjected to bending, with images taken at low (a_1–c_1) and high (a_2–c_2) magnifications.

was reduced by at least 30% (from 4.8 GPa to 3.3 GPa) once the knuckle was formed. These results clearly indicate that knuckle formation (rather than kink band formation) induces a permanent irreversible damage in the fiber. For this reason, this investigation was focused in the critical compressive strain to form a knuckle rather than in the compressive strain required to initiate the kink bands, and the compressive strength of PBO fibers was determined from the critical bending strain to form a knuckle.

To get more insight into the micro-mechanism of kink-band propagation and knuckle formation, several fibers were cross-sectioned using a focused ion beam. The longitudinal cross-section across one of these knuckles is shown in Figure 5. The layer of Pt was deposited on the surface to protect the fiber during milling. The strikes (vertical lines) in Figure 5(c) are a well known curtaining effect that occurs during the ion milling process. Two kink bands, with opposite inclination angles, are clearly

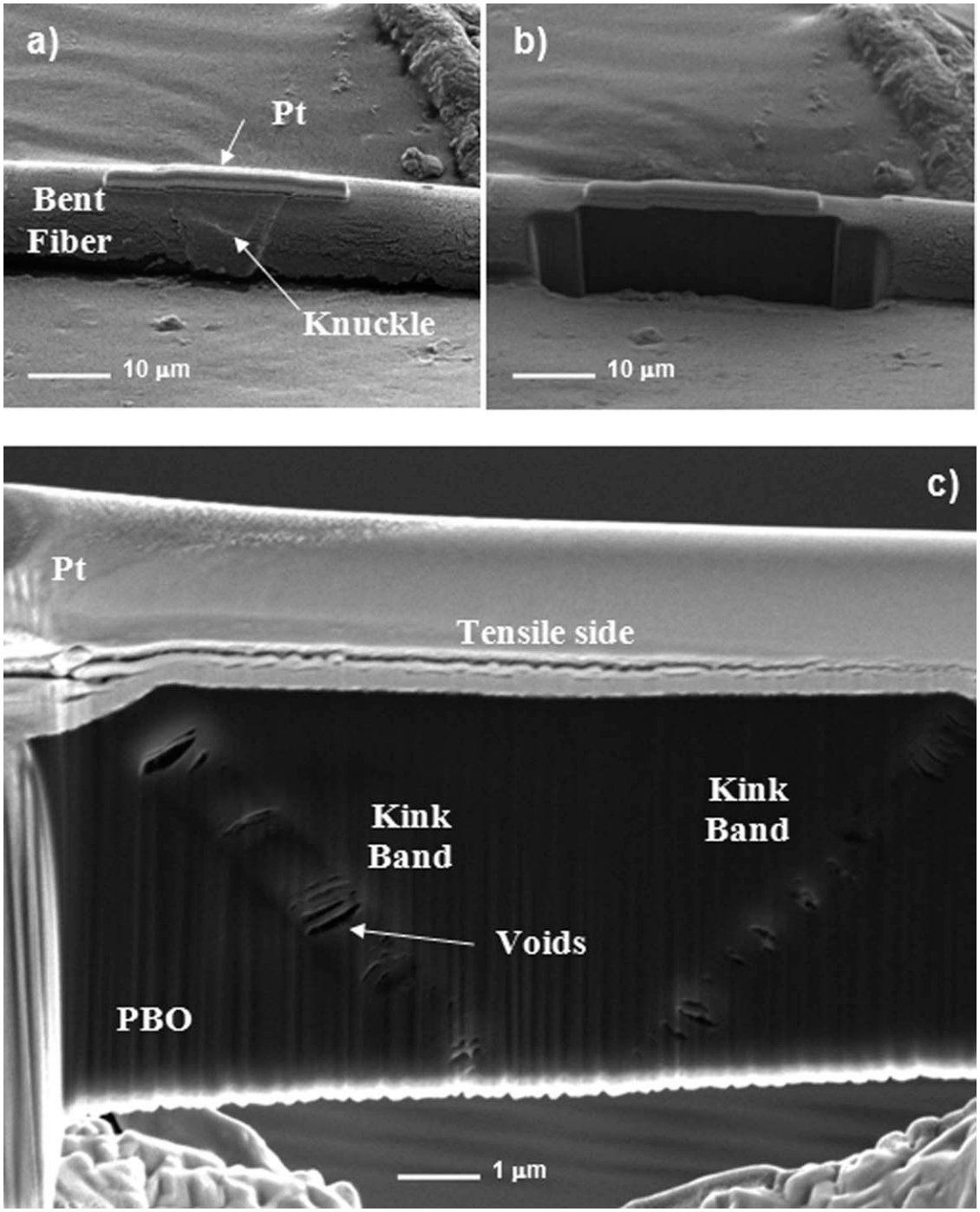

Figure 5 SEM images of a knuckle formed in a PBO fiber. (a) Knuckle prior to milling the longitudinal cross-section (Pt is deposited on the fiber surface to protect the fiber during milling). (b) Knuckle after the milling process. (c) Cross-section showing the two intersecting kink bands.

observed. Unfortunately, it was not possible to obtain a cross-section right across the fiber axis, and the image does not show the point of intersection of the two kink bands. It does provide, however, very interesting information inherent to the mechanism of kinking. Firstly, the kinks initiated at the compressive side of the bent fiber (not seen in the image) and are formed by two distinct kink boundaries that

TABLE I
Kink Band Angle, Diameter (Mean Value), and Critical Compressive Strain (ε_c) for Z, ZO4, and ZN4 Fibers

	Z	ZO4	ZN4
Kink band angle (°)	62 ± 8	66 ± 4	61 ± 4
Diameter (μm)	13.6 ± 1.0	13.1 ± 0.8	13.0 ± 0.6
ε_c (%)	1.7 ± 0.1	1.9 ± 0.5	2.4 ± 0.5

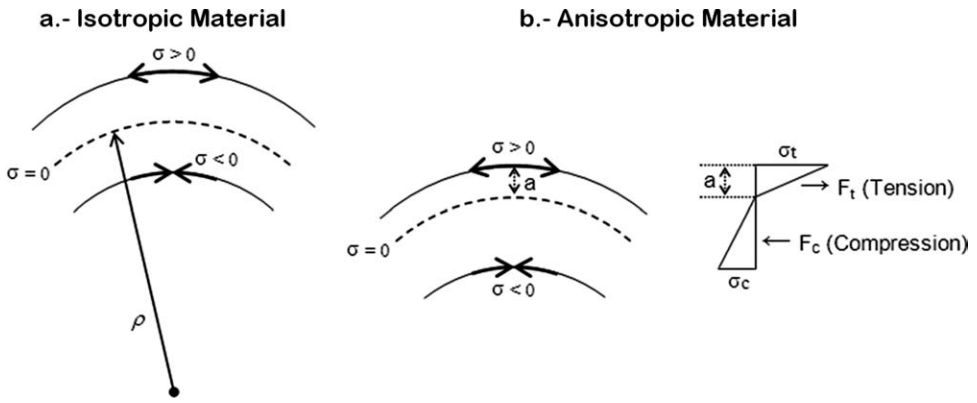

Figure 6 Stresses induced by bending in (a) isotropic and (b) anisotropic fibers.

accommodate the change in orientation of the polymeric chains in the kinked region. The width of the kinks w in this case was between 300 nm and 400 nm, although this is not always the case, as it depends on the amount of bending imposed. The angle at which the crystallites are sheared in this kink band region is of the order of 20–30° which is complimentary with the kink-band angle of 69° reported in this work. This corroborates the observation carried out before by Leal et al. in the case of M-5 fibers.[24] Secondly, voids are formed within the kink band by lateral splitting between the polymeric chains, as a result of the kinking process. And thirdly, voids are found within the fiber, where the kink boundaries are sharp, while no voiding between microfibrils is observed near to the fiber surface and the kink boundaries are more diffuse in this region. This is an indication of the structural differences between the skin and the core in PBO fibers,[25] with the skin displaying less microvoids, which has an influence on the process of kink band formation and propagation.

This sequence of events, resulting in the formation of a knuckle across the fiber cross-section, was identical for both treated and untreated fibers. Kink bands started to form at the compressive inner surface and propagated through the entire cross-section until a knuckle was formed. The angle between the kink band and the fiber axis was measured for all fibers and the average values are listed in Table I. They compare reasonably well with previous results (68°[1,9] and 69°[8]) where the PBO fiber was synthesized in the laboratory. Our SEM observations support the idea that a kink band is initiated on the fiber surface and then propagates along a well-defined plane.[9,11]

As indicated above, the curvature of the fiber subjected to bending is homogeneous prior to the formation of a knuckle and it is possible to measure the radius of curvature, ρ, from the SEM micrographs as the radius of the circumference which circumscribes the bent fiber [Fig. 6(a)]. The corresponding compressive strain at the fiber surface can be obtained from ρ following the Navier hypothesis for an elastic beam deformed in bending. It is assumed that the beam sections perpendicular to the beam axis remain straight after deformation, and thus the elastic strain varies linearly across the beam depth. If the material is isotropic (equal elastic modulus in tension and compression), the neutral axis is located at the center of the beam and the maximum strains in tension (ε_t) and compression (ε_c) are equal and given by:

$$\varepsilon_t = \frac{R}{\rho} \quad \text{and} \quad \varepsilon_c = \frac{-R}{\rho} \tag{1}$$

where R is the fiber radius. However, PBO is highly anisotropic, the tensile elastic modulus $E_t = 230$ GPa being much higher than the compressive one $E_c =$

TABLE II
Compressive Strength of PBO Fiber Obtained from Different Studies

Compressive strength (GPa)	Ref.	Testing method
0.190 GPa	5	DILA + tip indenter[a]
0.221 GPa	15	Recoil method[a]
0.300 GPa	26	Raman spectroscopy[a]
0.561 GPa	27	Bending beam method[b]
0.600[c] GPa	28	Twisting tester (KES-G7)[b]
1.24[d] GPa	This work	Bending test[a]

[a] Single filament.
[b] Bundle of fibers.
[c] At 0.44% strain.
[d] Estimated value for 1.7% strain and using $E_c = 73$ GPa.[5]

TABLE III
Tensile Properties of Z, ZO4, and ZN4 Samples

	Tensile strength (GPa)	Strain (%)	E (GPa)
Z	4.8 ± 0.9	2.2 ± 0.3	230 ± 40
ZO4	4.5 ± 0.6	2.0 ± 0.2	233 ± 24
ZN4	4.3 ± 0.9	1.8 ± 0.3	249 ± 32

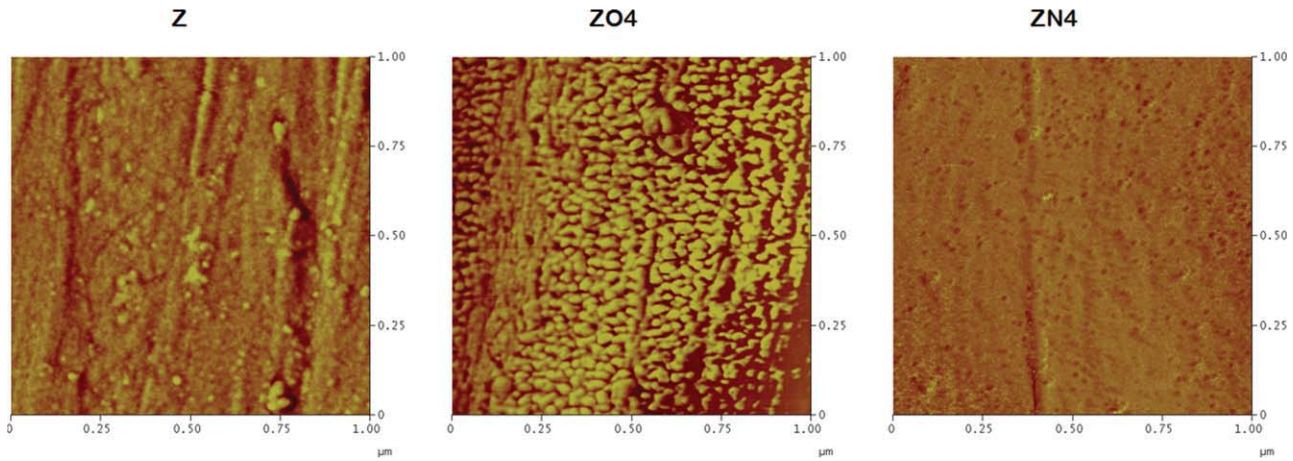

Figure 7 Tapping mode AFM phase contrast images of Z, ZO4 and ZN4.[20,33] [Color figure can be viewed in the online issue, which is available at wileyonlinelibrary.com.]

73 GPa.[5,24] As a result, the neutral axis is shifted from the center of the fibers towards the tensile zone [Fig. 6(b)], and eq. (1) should be modified to compute the maximum compressive strain at the fiber surface according to

$$\varepsilon_c = \frac{-2R + a}{\rho} \tag{2}$$

where a can be determined from the mismatch in the elastic moduli by imposing the condition that the net force on the beam section due to the contribution of tensile and compressive stresses should be zero. Mathematically, this is established by the following integral equation

$$\int_0^a \sigma_t dA_t = \int_a^{2R} \sigma_c dA_c \tag{3}$$

where σ_t and σ_c are, respectively, the tensile and compressive stresses on the fiber cross-section and, A_t and A_c, the tensile and compressive cross-sectional areas [Fig. 5(b)].

The critical compressive strain, ε_c, for knuckle formation was calculated according to eq. (2) from the critical curvature radius right before the formation of the knuckle. The average value corresponding to the as-received fibers is presented in Table I. The compressive strength of the as-received fibers Z can be estimated as the product of the critical compressive strain (1.7 ± 0.1%) times the fiber compressive elastic modulus E_c (Table II), leading to 1.24 GPa. This value is one order of magnitude higher than those reported elsewhere and listed in Table II, and the differences arise from the criteria used to define the compressive strength. In the different tests reported in the literature,[5,15,26–29] the compressive strength is related to the nucleation of kink bands, while the compressive strength in our case was dictated by the development of irreversible damage by the intersection of two kink bands to form a knuckle. As discussed elsewhere,[23] this is a typical controversy motivated by the fact that most studies use optical microscopy to detect the onset of kink-band formation and this is assumed to represent the compressive failure strain, while in most cases kinks are completely form prior to compression failure.

Table I also includes the critical compressive strains measured in the plasma-treated samples. While the oxygen treatment led to a slight increase (10%) in the critical compressive strain, the nitrogen-plasma treatment induced a dramatic improvement of the order of 40%. In addition, the plasma treatments had negligible effects on other bulk properties of the fibers, such as the tensile strength of the fiber (Table III). To the best of our knowledge, this is the first time that such an improvement is demonstrated in the compressive strength of PBO fibers without compromising the tensile strength.

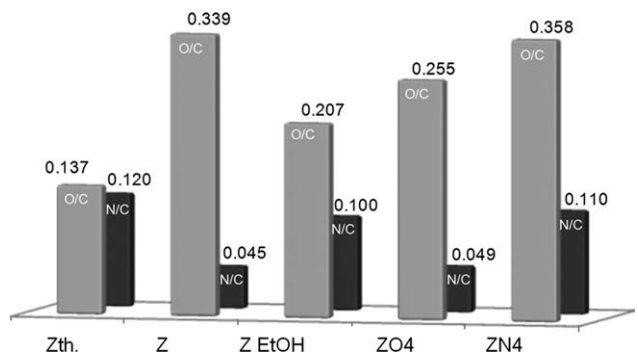

Figure 8 O/C and N/C atomic ratios corresponding to Z theoretical (Zth) and PBO fiber washed with Ethanol (Z EtOH)[31] together with those determined by XPS: Z, ZO4, and ZN4 samples.

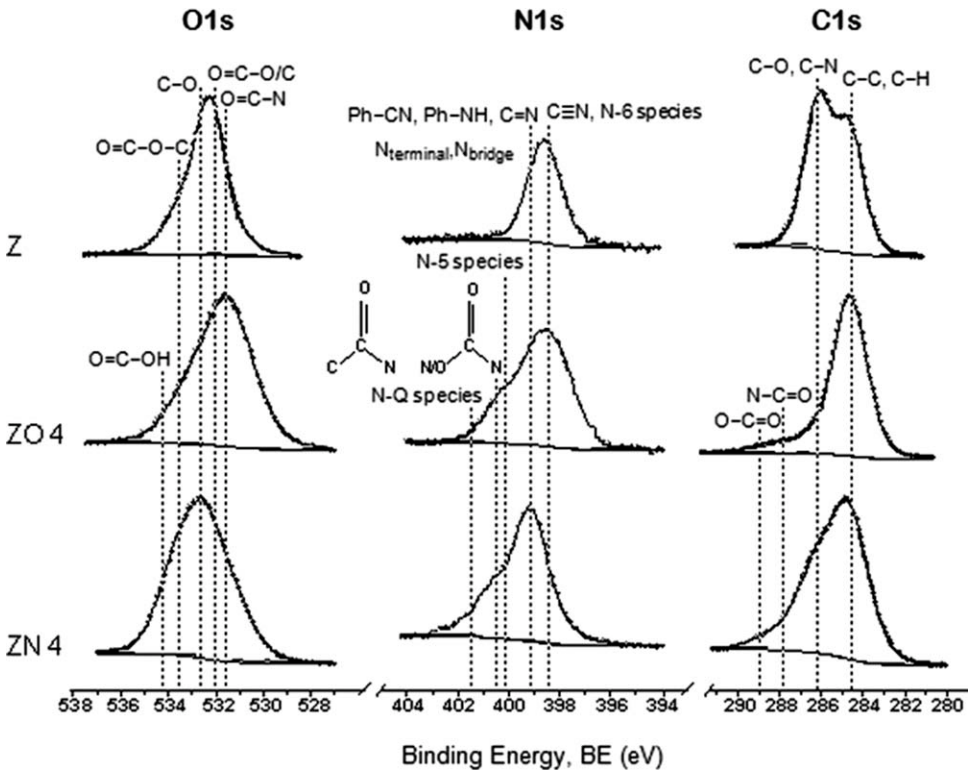

Figure 9 O1s, N1s, and C1s spectra of Z, ZO4, and ZN4 fibers.

Morphological and chemical changes induced by the plasma treatments

The effects of the different plasma treatments on the surface morphology can be observed in the AFM images of Figure 7. Both in the case of ZO4 and ZN4, the axial nanofibrillar structure of untreated PBO was substituted by irregular domains (rounded and globular nanostructures) which coexisted with several areas arranged more or less parallel to the fiber axis.[20,30] The loss of certain degree of anisotropy on the surface fiber upon plasma treatment might be an indication of morphological changes leading to a higher resistance against chain sliding, which contributes to delay the kink band formation. However, this reduction in the degree of anisotropy occurred both for ZO4 and ZN4 fibers and therefore cannot solely explain the radical improvement observed for the nitrogen plasma as opposed to the oxygen plasma. On the contrary, XPS results provided evidence of substantial differences between ZO4 and ZN4.

The atomic ratios, as determined by XPS, are shown in Figure 8. It was found that the O/C and N/C ratios of ZN4 were higher than those of the Z and ZO4 fibers. In the case of the oxygen plasma treatment, the O/C ratio diminished approximately by 25% with respect to the unmodified fiber (Fig. 8). However, it should be noticed that the atomic ratio of the as-received fiber was much higher than the theoretical one calculated from the molecular structure of PBO monomer unit (Fig. 1), labeled as Zth in Figure 8. The high O/C ratio in Z is very likely a result of surface contamination by processing substances (i.e., solvents wastes) because it has been demonstrated that the O/C ratio of the PBO surface cleaned with polar solvents was very similar than that calculated for Zth (Fig. 8).[31,32]

The reduction of the O/C ratio in the ZO4 fiber was probably due to the cleaning effect that took

TABLE IV
XPS Assignations for C1s and N1s Core Levels

	Chemical bonds	BE (eV)
C1s core level	C—C, C—H, $C_{\varnothing}$	284.6[39]
	C—N, C—O	286.3[38]
	C=N	287.0[36]
	CONH–	287.8[37]
	HO—C=O	289.0[38,40]
N1s core level	N-6 (pyridinic)	398.3[41]
	C≡N	398.5[36,40]
	C—N	398.5[42,43]
	C=N	399.1[36,42]
	Ph—CN, Ph—NH—	399.2[41]
	N-5 (pyrrolic and/or pyridonic)	400.1[41]
	—NCOO—, —NCON—, N—O	400.5[36]
	HN—C=O	400.7[43]
	N-Q (quaternary species)	401.5[41]
O1s core level	HN—C=O	531.6[37]
	—O—C=O	532.2[21]
	C=O	532.3[21]
	C—O—C	532.6[21]
	C—OH	532.9[21]
	C—O—C=O	533.6[21]
	HO—C=O	534.3[40]

place during the oxygen plasma treatment. Firstly, the oxygen plasma usually results in a removal processes induced by physical etching whose rate increases with the reactive species density[30] and consequently, the degree of dissociation. On the other hand, Chen et al. proved that, for oxygen plasma treated PBO fibers, the O/C ratio increased as the plasma power increases until a certain value, after which the O/C ratio started to diminish.[32] They concluded that the oxygen plasma introduces polar groups onto the PBO surface, which are decomposed at higher powers due to etching reactions.[32] In this sense, the AFM images of Figure 7 demonstrate that, for ZO4, the oxygen plasma induces a cleaning effect removing contaminant substances related to processing wastes, while the anisotropy inherent to the starting material is still observed.[33]

In the case of ZN4, the O/C ratio increased slightly ($\sim$ 5%) with respect to the untreated material whereas N/C increased more than twice, as could be expected after the nitrogen plasma treatment (Fig. 8). In general, more energy is necessary to generate reactive species with the nitrogen plasma than with the oxygen plasma[18,34] because the dissociation and ionization energies of the nitrogen species are higher than those of the oxygen species. In addition, the emitted UV radiation from the nitrogen plasma treatment is important and sufficient to break polymeric bonds.[34] In this way, the bond breaking can lead to the formation of new functional groups without incorporation of new species. It is difficult to predict in polymers containing heteroatoms (O and N) whether the incorporation of functional groups is due either to the incorporation of species generated in the plasma treatments and/or bonds breaking in the polymer structure. That is to say, the radicals formed during the plasma treatment could be stabilized reacting with species present in the discharge chamber (previously volatilized), participating in crosslinking reactions between polymeric segments and/or stabilizing with atmospheric species during the post-treatment. Such post-plasma reactions are usually attributed to the existence of long-live radicals' sites onto the surface. This could justify that under identical plasma process parameters, the atomic ratios are higher for ZN4 than that ZO4 (Fig. 8).

Figure 9 shows the O1s, N1s, and C1s profiles obtained for each sample. With the plasma treatments, the shape of the C1s profiles is rather different than for the unmodified sample Z. The first contribution, placed at 284.6 eV and which is taken as a reference, is attributed to the C=C (Csp^2, aromatic carbon).[21] The second one at 286.1 eV, according to the molecular structure of PBO (Fig. 1), should be less intense; i.e., the monomer unit is formed by 12 C=C aromatic bonds, 1 C—C bond, 4 C—O bonds, 2 C=N, and 2 C—N. Therefore, as the proportion of C—C bonds (aromatic or not) is the highest, it is expected that the contribution centered at 284.6 eV should be the highest. Lange et al. obtained a carbon profile peak for an aramid fiber with finish, very similar than that obtained in this work for Z.[35] They attributed the behavior observed for the contribution placed at 286.1 eV to the finish C—O bonds.[35] As the O/C ratio of the PBO fiber diminishes considerably using a polar solvent (named as Z EtOH in Fig. 8),[31] the contaminant substances detected on Z surface may be responsible for the high O/C ratio obtained (Fig. 8). With the plasma treatments, the second contribution centered about 286.1 eV diminishes and the shape of C1s widens towards higher BE side (i.e., above 288.2 eV, Fig. 9). Moreover, the O1s and N1s profiles are broad and appear to be asymmetric on the higher BE side. Additionally, O1s and N1s displace 0.3 eV towards higher BE for ZN4 and 0.7 eV towards smaller BE for ZO4. Therefore, the signal observed at 288.2 eV for C1s profiles corresponding to ZO4 and ZN4 may be associated to oxidized carbon like C=N,[36] HN—C=O[37] and/or HO—C=O,[38] according to the literature related to organic polymers and functionalized carbon materials (summarized in Table IV).

Another significant variation respect to the Z sample is observed at the N1s peak. This peak displays a shoulder on the higher binding energy side and a widening of the N1s spectra as a result of the plasma treatments. The contribution of higher binding energy can be attributed to: (i) C=N or O—N[36,42]; (ii) N-5 polycondensation systems[41]; and/or (iii), —NCOO—, —NCON—, —N—O,[36] and/or —HN—C=O,[43] taking into account the appearance of the oxidized component for the C1s core level. Moreover, as the N1s spectrum of ZN4 is more shifted towards higher binding energies than ZO4, the presence of quaternary species (N-Q) formed due to hydrogen bonds between the N-5 species and the hydrogen atoms of neighbor chains cannot be discarded.[44,45] The results thus would indicate more crosslinking between polymeric chains in the case of the nitrogen plasma treated fibers, which would lead to higher resistance against chain sliding and contribute to delay in the kink band formation.

DISCUSSION

The detailed observations of the longitudinal cross-section of the kinked fibers by FIB and SEM allow as to draw some interesting conclusions about the process of kink band initiation and propagation, which is the mechanism responsible for the compressive failure of PBO fibers. Figure 10(a) shows a schematic illustration of the process of kink band initiation. Kink bands are initiated at the compression surface

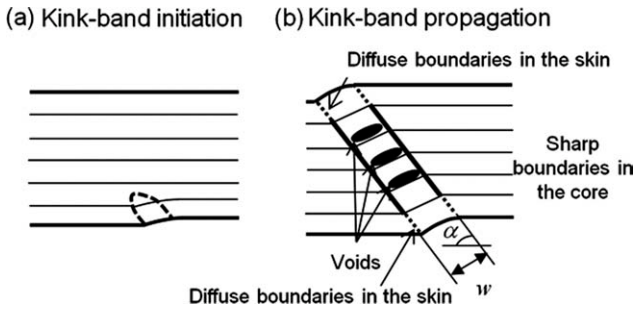

Figure 10 Schematic illustration showing the (a) initiation and (b) propagation of a kink-band. Kink-bands generate at the compressive surface and propagate across the entire cross section. Kink-bands generate at the compressive surface and propagate across the entire cross-section. The appearance of the kink bands is different at the skin and at the core. Kink boundaries are diffused at the skin, while they are sharp within the core, where interchain voids develop due to the weak interaction between polymeric chains.

of the bent fiber. No conclusion can be drawn from the observations on the exact initiation mechanism, which could be either due to a buckling or a shear instability, although the latter theory has more support in crystalline materials which fail by kinking in compression.[46] Once formed, the kink rapidly propagates across the entire cross-section of the fiber forming two distinct kink boundaries, as illustrated in Figure 10(b). Our FIB observations show differences in the nature of the kink boundaries between the fiber skin and the core. They are sharp at the core, and this is associated with lateral splitting between ordered polymeric chains leading to the formation of voids aligned with the chains. These voids are formed due to the weak interaction between the polymeric chains and are confined by the kink boundaries. However, the kink boundaries are diffused at the skin and no voids are formed, which is consistent with the higher density of the skin as compared with the fiber core.[25] The facts that kink bands initiate at the surface and that the kink boundaries are diffused at the skin with no voiding between polymeric chains indicate that the fiber surface plays a major role in the process of kink band formation and propagation. Therefore, any surface treatment that promotes crosslinking between polymeric chains, such as plasma treatments, has the potential to modify the compressive strength of the fibers.

The SEM studies also allow to draw some interesting conclusions about the sequence of events that leads to the development of permanent damage during bending. Such sequence of events is schematically illustrated in Figure 11. Upon bending, parallel and regularly spaced individual kink bands are nucleated along the fiber starting at the compression surface of the fiber, at each side of the bent fiber segment [Fig. 11(a)]. These kink bands disappear on unbending [Fig. 11(b)] and do not modify the fiber tensile strength. Therefore the appearance of individual kink bands cannot be taken as a criterion to determine the compressive strength of the fibers. Further bending increases the number of kink bands until two opposing kink bands intersect at approximately the center of the bent fiber segment [Fig. 11(c)]. The intersection of these two kink bands produces a "V" shape defect that we refer to as a knuckle. The intersection of kink bands causes further void formation, bulging, and irregular bending of the polymeric chains and constitute an irreversible type of damage that do not disappear upon unloading. Moreover, the strain is localized at the knuckle upon further bending and unbending. We have corroborated that knuckled fibers display a reduction in tensile strength of at least 30%, which could be even higher if the knuckled fiber is subjected to fatigue load. Thus, the compressive strain necessary to create a knuckle is a more appropriate criterion than the strain for kink band initiation to define the compressive strength of PBO fibers.

Regarding the effect of surface plasma treatments, the results show a radical improvement in the critical compressive strain needed to form a knuckle in fibers treated with nitrogen plasma, while this is not the case in fibers treated with oxygen plasma considering the dispersion of the experimental data (Table I). The mechanisms of kink band formation and propagation were the same in all cases as well as the measured kink band angles. On the contrary, previous studies by Leal et al.[47] showed that an increase

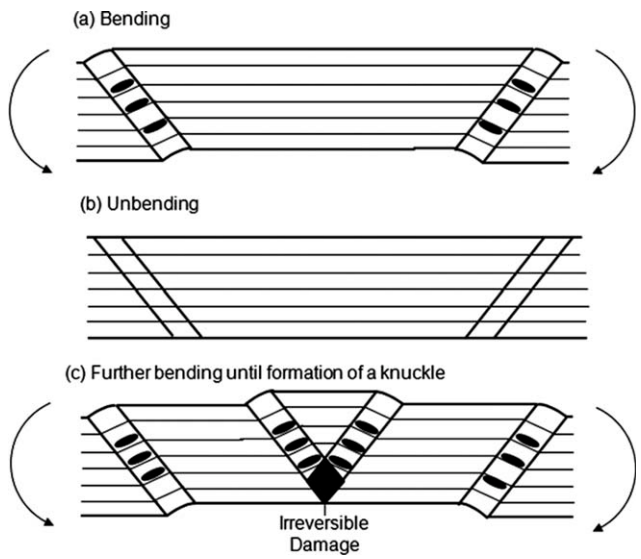

Figure 11 Schematic illustrations showing (a) the formation of kink bands during bending; (b) elimination of kink bands upon bending showing the reversibility of the process; and (c) development of further kink bands with further bending until two intersecting kink-bands form a knuckle. The process of knuckle formation is not reversible upon unbending, and leads to permanent damage.

in intermolecular bonding in M5 fibers also changes the kink-band angle but in that case the treatment affected the entire volume of the fiber. The fact that the kink band angle is not modified in our case seems to indicate that the plasma treatment only affects the outermost surface of the fiber. In this respect, it is expected that any surface modification that enhances the lateral interaction between polymeric chains should be beneficial in delaying the formation and propagation of kink bands and this can be achieved in different ways. For instance, McGarry and Moalli showed that coating of the surface fiber with a ceramic material improved the compressive strength due to the resistance provided by the coating to the kink band development.[11] However this was accompanied by considerable loss in the tensile strength of the fibers. In the case of plasma treatments, only the uppermost layers of the material were altered and hence the tensile strength is not affected by the treatment.

XPS results provide evidence of substantial variations induced by the oxygen and nitrogen plasma treatments that can explain the different behaviors of ZO4 and ZN4 fibers. The BE shifts detected for the maximum of O1s and N1s profiles with the plasma treatments (towards smaller BE for ZO4 and at higher BE for ZN4, see Fig. 7) imply that some of the electron density on the heteroatoms (N and O) has been drawn in the case of ZN4. However, as the maximum of O1s and N1s is placed 1 eV towards smaller BE for ZO4, the electron-donor capacity of the heteroatoms is higher for ZO4 than ZN4. In addition, the contribution placed at 286.1 eV for ZO4 has diminished considerably respect to Z; i.e., it is not practically detected on C1s spectrum (Fig. 8). On the other hand, the C1s spectrum is widened up to 288 eV which means that oxidized functional groups such as amides, esters and/or carboxylic acids develop with the oxygen plasma treatment. The presence of these groups justifies the shoulder observed on N1s profile for ZO4 which could be associated with NCOO and NCON groups in which the carbon is very oxidized. Finally, N-5 and N-Q species cannot discarded (Fig. 9), although the contribution of N-Q species is not as important as in the case of ZN4 (Fig. 9, see N1s profiles of ZO4 and ZN4). In agreement with previous reports,[19,33] these observations indicated that post-treated ZO4 surfaces absorb water molecules when exposed to air. Therefore, surface swelling can be developed as result of hydrogen bonds between ZO4 heteroatoms (O and N) of the functional groups (amides, carboxylic acids, alcohol and/or amines groups) and the water molecules present in the air.

On the contrary, the ZN4 surface does not undergo swelling during the post-treatment.[19] According to the next binding energy ranges centered at 398.0–398.4 and 400.0–400.7 eV for N1s, it is well established that the nitrogen is in an environment of sp^3 and sp^2 carbons, respectively.[48] The N1s spectrum of ZN4 is displaced towards higher binding energies with respect to Z and ZO4 (Fig. 9), and this is indicative that the chemical structures developed are more rigid because the bonds in sp^2 configuration have lost one degree of freedom (the bonds cannot rotate). In addition, this assumption is supported by the possible formation of quaternary species (N-Q), as evidenced in the N1s spectrum of ZN4 (Fig. 9), which are the result of hydrogen bonds formed between nitrogen of N-5 species and neighboring hydrogen atoms. The presence of polycondensed systems onto ZN4 surface bonded by hydrogen bonds evidences crosslinking between polymeric chains. This would result on a higher resistance against chain sliding for the ZN4 structure, justifying the improvement of the critical compressive strain for knuckle formation.[39,40,49]

CONCLUSIONS

The mechanical behavior in compression of PBO fibers was studied by means of *in situ* bending tests carried out inside a scanning electron microscope. The critical strain for the nucleation of a knuckle (made up by the intersection of two kinks bands with opposite orientation) was carefully determined from the fiber curvature, taking into account the fiber anisotropy. It has been demonstrated that knuckles, contrary to isolated kink bands, constitute an irreversible type of damage that has a marked influence of the residual tensile strength of the fiber.

Tests were carried out in as-received fibers as well as on fibers subjected to surface plasma treatments in either nitrogen or oxygen atmosphere. While the micromechanisms of kink-band nucleation and formation were the same in all cases, the nitrogen plasma treated fibers presented a marked improvement ($\approx$ 40%) in the critical compressive strain for knuckle formation while the tensile strength of the fibers was maintained. Careful analysis of the morphology and chemistry of the fiber surface after the plasma treatments suggested that the improvement may be caused by the crosslinking between polymeric chains at the fiber surface.

The use of the FIB system at CEIT in San Sebastian, Spain is gratefully acknowledged. The results presented are protected by patent application P201001483 (19 November 2010).

References

1. Martin, D. C.; Thomas, E. L. J Mater Sci 1991, 26, 5171.
2. Flory, J. In Oceans 96 MTS/IEEE Supplementary Proceedings, Piscataway, New Jersey, 1996; p 93.

3. Yamashita, Y.; Kawabata, S.; Kido, A. Adv Compos Mater 2001, 10, 275.
4. Elices, M.; Lorca, J. Fiber Fracture; Elsevier, Oxford, 2002; p 393.
5. Andreas Leal, A.; Deitzel, J. M.; Gillespie, J. W., Jr. Compos Sci Technol 2007, 67, 2786.
6. Afshari, M.; Sikkema, D. J.; Lee, K.; Bogle, M. Polym Rev 2008, 48, 230.
7. Chae, H. G.; Kumar, S. J Appl Polym Sci 2006, 100, 791.
8. Chau, C. C.; Blackson, J. Im, J. Polymer 1995, 36, 2511.
9. Huh, W.; Kumar, S.; Adams, W. E. Polym Eng Sci 2003, 43, 684.
10. Hobbs, R.; Overington, M.; Hearle, J. W. S.; Banfield, S. J. J Text Inst 2000, 91, 335.
11. Mc Garry, F. J.; Moalli, J. E. Polymer 1991, 32, 1816.
12. Kumar, S.; Dang, T. D.; Arnold, F. E.; Bhattacharyya, A. R.; Min, B. G.; Zhang, X.; Vaia, R. A.; Park, C.; Adams, W. W.; Hauge, R. H.; Smalley, R. E.; Ramesh, S.; Willis, P. A. Macromolecules 2002, 35, 9039.
13. Lin, H.; Huang, Y.; Wang, F. Int J Mol Sci 2008, 9, 2159.
14. So, Y. H. Prog Polym Sci 2000, 25, 137.
15. Dean, D. R.; Husband, D. M.; Dotrong, M.; Wang, C. S.; Dotrong, M. H.; Click, W. E.; Evers, R. C. J Polym Sci Part A Polym Chem 1997, 35, 3457.
16. De Teresa, S. J.; Porter, R.; Farris, R. J. J Mater Sci 1988, 23, 1886.
17. Argon, A. S. In Treatise on Materials Science and Technology; Academic Press: New York and London, 1972; p 79.
18. Hollahan, J. R.; Bell A. T. Techniques and Applications of Plasma Chemistry; Wiley & Sons: New York, 1974.
19. Tamargo-Martínez, K.; Martínez-Alonso, A.; Montes-Morán, M. A.; Tascón, J. M. D. J Comp Sci Tech 2011, 71, 784.
20. Tamargo-Martínez, K. Ph.D. Dissertation, University of Oviedo (Oviedo, Spain), 2007.
21. Beamson, G.; Briggs, D. High Resolution XPS of Organic Polymers : The Scienta Esca300 Database; Wiley: Chichester, 1992.
22. Wagner, C. D.; Davis, L. E.; Zeller, M. V.; Taylor, J. A.; Raymond, R. H.; Gale, L. H. Surf Interface Anal 1982, 3, 211.
23. Lynn Vezie, D. Ph.D. Dissertation, Massachusetts Institute of Technology (Boston, USA), 1993.
24. Andres Leal, A.; Deitzel, J. M.; Gillespie, J. W., Jr. J Compos Mater 2009, 43, 661.
25. Kitagawa, T.; Murase, H.; Yabuki, K. J Polym Sci Part B Polym Phys 1998, 36, 39.
26. So, C. L.; Bennett, J. A.; Sirichaisit, J.; Young, R. J Plast Rubber Compos 2003, 32, 199.
27. Toyobo. Technical information "PBO Fiber Zylon"; Toyobo Co Ltd., Osaka, Japan, 2001.
28. Yamashita, Y.; Kawabata, S.; Minami, H.; Okada, S.; Tanaka, A. In Proceedings of the 30th Textile Research Symposium; Mt. Fuji in the New-Millennium, Shizuoka 2001; p 219.
29. Kozey, V. V.; Jiang, H.; Mohta, V. R.; Kumar, S. J Mater Res 1995, 10, 1044.
30. Ferreira, C. M.; Moisan, M.; Zakrzewski, Z. In Microwave Excited Plasmas, Plasma Technology, 1st ed.; Moisan, M., Pelletier, J., Eds.; Elsevier: Amsterdam, 1992; Vol. 4, Chapter 3.
31. Tamargo-Martínez, K.; Villar-rodil, S.; Paredes, J. I.; Martínez-Alonso, A.; Tascón, J. M. D.; Montes-Morán, M. A. Macromolecules 2003, 36, 8662.
32. Chen, P.; Zhang, C.; Zhang, X.; Wang, B.; Lei, W.; Lei, Q. Appl Surf Sci 2008, 255, 3153.
33. Tamargo-Martínez, K.; Martínez-Alonso, A.; Gracia, M.; Paredes, J. I.; Tascón, J. M. D.; Montes-Morán, M. A. In Proceedings of V International Conference on Science and Technology of Composites Materials; San Sebastián, 2009; p 1105.
34. Chan, C. M.; Ko, T. M. Surf Sci Rep 1996, 24, 1.
35. De Lange, P. J.; Mäder, E.; Mai, K.; Young, R. J., Ahmad, I. Compos A 2001, 32, 331.
36. Gerenser, L. J.; Grace, J. M., Apai, G.; Thompson, P. M. Surf Interface Anal 1999, 9, 12.
37. Chapell, P. J. C., Williams, D. R., George, G. A. J Colloid Interface Sci 1990, 134, 385.
38. Wang, Q.; Kaliaguine, S.; Ait-Kadi, A. J Appl Polym Sci 1993, 48, 121.
39. Cuesta, A.; Martínez-Alonso, A.; Tascón, J. M. D.; Bradley, R. H. Carbon 1990, 35, 967.
40. Clark, D. T.; Cromarty, B. J.; Dilks, A. J Polym Sci Part A Polym Chem 1978, 16, 3173.
41. Hueso, J. L.; Espinós, J. P.; Caballero, A.; Cetrino, J.; González-Elipe, A. R. Carbon 2007, 45, 89.
42. Dementjev, A. P.; De Graaf, A.; Van de Sanden, M. C. M.; Maslakov, K. I.; Naumkin, A. V.; Serov, A. A. Diam Relat Mater 2000, 9, 1904.
43. Ruelle, B.; Peeterbroeck, S.; Gouttebaron, R.; Godfroid, T.; Monteverde, F.; Dauchot, J. P.; Alexandre, M.; Hecqb, M.; Dubois, P. J Mater Chem 2007, 17, 157.
44. Boudou, J. P.; Parent, Ph.; Suárez-García, F.; Villar-Rodil, S.; Martínez-Alonso, A.; Tascón, J. M. D. Carbon 2006, 44, 2452.
45. Vehovar, L.; Vehovar, A.; Metikos-Hukovic, M.; Tandler, M. Mater Corros 2002, 53, 316.
46. Molina-Aldareguia, J. M.; Emmerlich, J.; Palmquist, J.-P., Jansson, U.; Hultman, L. Script Mater 2003, 49, 155.
47. Andres Leal, A.; Deitzel, J. M.; McKnight, S. H.; Gillespie, J. W., Jr. Polymer 2009, 50, 2900.
48. Zheng, W. T.; Xing, K. Z.; Hellgren, N.; Lögdlund, M.; Johansson, A.; Gelivs, U.; Salaneck, W. R.; Sundgren, J.-E. J Electron Spectrosc Relat Phenom 1997, 87, 45.
49. Cuong, N. K.; Dao, T. T.; Hung, N. T. In Proceedings of the Ninth Asia Pacific Physics Conference; Vietnam, 2004, p 747.